Journal of Nuclear Materials 397 (2010) 1–7

Contents lists available at ScienceDirect

Journal of Nuclear Materials

journal homepage: www.elsevier.com/locate/jnucmat

# Ab-initio calculations and phase diagram assessments of An–Al systems (An = U, Np, Pu)

D. Sedmidubský [a,b,*], R.J.M. Konings [a], P. Souček [a]

[a] European Commission, Joint Research Centre, Institute for Transuranium Elements, Post Box 2340, D-76125 Karlsruhe, Germany
[b] Institute of Chemical Technology, Technická 5, 166 28 Prague, Czech Republic

ARTICLE INFO

*Article history:*
Received 6 August 2009
Accepted 26 November 2009

ABSTRACT

The enthalpies of formation of binary intermetallic compounds $AnAl_n$ ($n = 2, 3, 4$, An = U, Np, Pu) were assessed from first principle calculations of total energies performed using full potential APW + lo technique within density functional theory (*WIEN2k*). The substantial contribution to entropies, $S^{\circ}_{298}$, arising from lattice vibrations was calculated by direct method within harmonic crystal approximation (*Phonon* software + *VASP* for obtaining Hellmann–Feynman forces). The electronic heat capacity and the corresponding contribution to entropy were estimated from the density of states at Fermi level obtained from electronic structure calculations. The phase diagrams of the relevant systems An–Al were calculated based on the thermodynamic data assessed from ab-initio calculations, known equilibrium and calorimetry data by employing the *FactSage* program.



## 1. Introduction

Pyrochemical methods for spent nuclear fuel reprocessing are nowadays subject of worldwide investigation as they represent a promising alternative to aqueous reprocessing techniques. In particular, advanced fuels containing minor actinides, such as metallic, nitride or carbide fuels, might be difficult to treat by hydrometallurgical processes due to their limited solubility in aqueous media, as well as due to limited radiation and thermal stability of the used organic solvents and extractants.

The most developed pyrochemical reprocessing technique is electrochemical separation of actinides from molten salt mixtures in which the spent fuel has been dissolved. In the process that is currently being developed in ITU[a], all actinides are selectively reduced from a molten LiCl–KCl electrolyte on a solid aluminium cathode, forming actinide–aluminium alloys by solid state reaction [1]. These intermediate products should subsequently undergo a chlorination and the respective actinide chlorides could then be easily separated from $AlCl_3$ taking use of a considerably higher volatility of the latter chloride.

During the electrodeposition, the respective $An^{3+}$ cation is reduced on the Al-electrode forming a solid $AnAl_n$ phase at a specific potential, where $n$ might be an integer for a stoichiometric intermetallic compound or real if a solid solution is formed. In the latter case the stoichiometry of the alloy is determined by both the activity of An in chloride electrolyte and the cathode potential. Since the characteristic reduction potentials of actinides differ appreciably from those of rare earths and other fission products, the electrochemical separation process can be conducted very effectively. Moreover, highly thermodynamically stable actinide alloys are formed during the process which prevents them from re-oxidation or other corrosive behavior.

It is obvious from what is mentioned above that the separation abilities of the electrorefining process as well at the subsequent conversion steps strongly depend on the thermodynamic properties of the formed An–Al alloys. Knowledge of their properties is thus of principal importance for the appropriate description and optimization of the processes involved in the depicted approach of spent nuclear fuel reprocessing.

The high temperature equilibrium data in U–Al and Pu–Al systems have been compiled by Kassner et al. [2,3] and the corresponding phase diagrams have been assessed, but not calculated. These are essentially based, except for a few modifications, on the previously published U–Al [4] and Pu–Al [5] diagrams. The U–Al phase diagram has been also recently assessed by Wang et al. [6] using a *CALPHAD* technique. By contrast, the phase diagram of Np–Al system is not available, however, the intermetallic compounds have been identified in the system and their melting behavior has been suggested based on thermal analysis experiments [7].

All three systems under study exhibit very similar phase relations with the dominating $AnAl_2$ phase crystallizing in the Laves $Cu_2Mg$ type (B15) structure. This most stable congruently melting compound is formed on the peritectic melting of $AnAl_3$

* Corresponding author. Address: Institute of Chemical Technology, Technická 5, 166 28 Prague, Czech Republic. Tel.: +420 220 444 122.
*E-mail address:* sedmidub@vscht.cz (D. Sedmidubský).

0022-3115/$ - see front matter © 2009 Elsevier B.V. All rights reserved.
doi:10.1016/j.jnucmat.2009.11.023

compound adopting the $AuCu_3$ type ($L1_2$). The less stable $AnAl_4$ ($UAl_4$ itself represents the structure type denoted as $D1_b$) decomposes peritectically into a liquid and $AnAl_3$ and forms the lowest eutectics with Al. Moreover, some particular features have been observed in Pu–Al system. First, $PuAl_3$ exists in three polymorphs differing in stacking of trigonal – ($PuAl_3$) – layers along the (0 0 1) direction – the low temperature rhombohedral form $PuAl_3$-9H, the intermediate hexagonal $PuAl_3$-6H and the high temperature cubic $PuAl_3$-3H described above. Second, two additional stoichiometric phases, tetragonal $Pu_3Al$ ($Pb_3Sr$ type) and a poorly characterized PuAl, as well as a relatively large range of $\delta$-Pu based solid solutions exist in the Pu-rich part of the phase diagram.

The direct measurements of thermochemical properties have been performed by solution calorimetry for $UA1_n$ [8,9] and $PuA1_n$ [10], and by high temperature adiabatic calorimetry for $UA1_n$ [11], resulting in highly exothermic values of enthalpies of formation, $\Delta_f H^{\circ}_{298}$, ranging from $-125$ kJ mol$^{-1}$ for $UAl_4$ to $-142$ kJ mol$^{-1}$ for $PuA1_2$. These data are in a relatively good agreement with those derived from high temperature emf measurements performed on $UA1_n$ [11,12] and $PuA1_n$ [4,13] compounds, which simultaneously provide negative values of entropies of formation. The heat capacities have been measured in sub-ambient temperature range for $AnAl_2$, An = U [14], Np [15], Pu [16], as well as for $AnAl_4$, An = U, Np [17]. Unfortunately, no entropies can be derived from these low temperature $C_p$ data for the comparison with the second law values based on the emf, since the available heat capacities do not cover the whole temperature range 0–298 K. The experimental enthalpies of formation and entropies are completely missing in the Np–Al system. It thus seems to be worth comparing the experimental information available for $UA1_n$ and $PuA1_n$ compounds with the enthalpies of formation and entropies resulting from current ab-initio calculation techniques and from the *CALPHAD* approach, as well as applying both methods on the Np–Al system.

## 2. Calculation details

The electronic structure calculations were performed within density functional theory (DFT) using the full-potential *WIEN2k* code [18] with APW + lo basis set and generalized gradient approximation (GGA, PBE96 parametrization scheme [19]) for exchange-correlation potential. The spin polarization with a simple ferromagnetic (FM) arrangement was considered for all phases. Such an assumption conforms the experimental evidence for $AnAl_2$ phases (see Section 3 below) and is also supported by our calculations performed for two different antiferromagnetic (AFM) arrangements of $NpA1_2$ phase. In this case, the FM structure is energetically favored by 80 meV compared to the AFM structure with all antiparallel nearest neighbors. The spin–orbit (S–O) coupling was included by applying the second variational procedure on the scalar-relativistic eigenstates. The basis was extended by relativistic $6p_{1/2}$ local orbitals centered at An atoms in all S–O calculations. The plane wave cut-off energy of 340 eV and the tetrahedron method with a typical $k$-mesh sampling density of 800 $k$-points Å$^3$ were used. The core configurations [Xe]$4f^{14}5d^{10}$ and [He]$2s^2$ were considered for An and Al atoms, respectively. These states are treated fully relativistically in *WIEN2k*. In order to treat the semicore states ($6s, 6p$ for An and $2p$ for Al), the corresponding local orbitals confined to muffin-tin spheres only were added. The well-proven muffin-tin radii $R_U = 2.45$ Å, $R_{Np} = R_{Pu} = 2.6$ Å and $R_{Al} = 1.8$ Å were selected in all calculated cases.

The crystallographic data of the An–Al intermetallic phases employed in ab-initio calculations are summarized in Table 1. The agreement of the calculated lattice parameters with the experimental structure data was tested by optimizing the unit cell volume on two example cases, $UA1_3$ and $NpA1_3$. For simple spin polarized calculations the difference between the experimental and optimized cubic lattice parameter $a$ was only $\sim -0.5\%$ and the corresponding energy difference did not exceed 0.6 kJ mol$^{-1}$. Although the inclusion of S–O coupling caused a more substantial underestimation of the lattice parameter ($\Delta a/a_{exp} \sim -1.1\%$) and the respective energy lowering by 5.3 and 6.5 kJ mol$^{-1}$, the impact on the resulting enthalpies of formation is not expected to be significant, since the S–O interaction is confined to An muffin-tin spheres of similar substances (the studied compounds and the reference elemental metals). Let us note that the lattice shrinkage due to S–O interaction is in fact compensated by strong correlations of $f$-electrons, which can be treated by GGA + U or hybrid functionals. These techniques are however difficult to apply for the prediction of enthalpies of formation as they involve adjustable parameters.

**Table 1**
Symmetry and lattice parameters used in *WIEN2k* [18], *Phonon* [21] and *VASP* [22] (SG – space group).

| | SG | $a$/Å | $b$/Å | $c$/Å | References |
|---|---|---|---|---|---|
| $UA1_2$ | $Fd\bar{3}m$ | 7.760 | 7.760 | 7.760 | [23] |
| $NpA1_2$ | $Fd\bar{3}m$ | 7.785 | 7.785 | 7.785 | [24] |
| $PuA1_2$ | $Fd\bar{3}m$ | 7.831 | 7.831 | 7.831 | [25] |
| $UA1_3$ | $Pm\bar{3}m$ | 4.253 | 4.253 | 4.253 | [26] |
| $NpA1_3$ | $Pm\bar{3}m$ | 4.260 | 4.260 | 4.260 | [27] |
| $PuA1_3$-3H | $Pm\bar{3}m$ | 4.262 | 4.262 | 4.262 | [28] |
| $PuA1_3$-9H | $R\bar{3}m$ | 6.150 | 6.150 | 21.10 | [29] |
| $UAl_4$ | *Imma* | 4.401 | 6.246 | 13.72 | [30] |
| $NpA1_4$ | *Imma* | 4.420 | 6.260 | 13.71 | [7] |
| $PuAl_4$ | *Imma* | 4.420 | 6.260 | 13.66 | [31] |

The simple structures of the constituent elements, $\alpha - A1(Fm\bar{3}m), \alpha$-$U(Cmcm), \gamma$-$Np(Im\bar{3}m)$ and $\delta$-Pu ($Fm\bar{3}m$) were considered as reference states for the evaluation of enthalpies of formation at $T = 0$ K from total energies obtained by DFT calculations. Since $\gamma$-Np and $\delta$-Pu refer to high temperature allotropes, their lattice parameters had to be optimized and the resulting enthalpies of formation were subsequently converted to the thermodynamic standard states referring to the respective $\alpha$-modifications using the known values of $\Delta H(Np_{\gamma\to\alpha}) = 10.9$ kJ mol$^{-1}$ and $\Delta H(Pu_{\delta\to\alpha}) = 12.5$ kJ mol$^{-1}$ [20].

The electronic contribution to the heat capacity was evaluated from the total density of states at Fermi level, $N(E_F)$ (summed over spin-up and spin-down channels), resulting from DFT calculations by assuming the simple Sommerfeld term

$$C_V^{el} = \mathbf{R}\frac{\pi}{3}k_B N(E_F)T. \quad (1)$$

The direct method as implemented in *Phonon* software [21] was applied to calculate the phonon density spectra (PDOS) and the corresponding contributions to thermodynamic quantities. The key property is indeed the heat capacity which can be computed from the phonon density of states, $g(\omega)$, by integrating over the populated phonon frequencies for a given temperature

$$C_V^{ph} = \mathbf{R}\int_0^{\omega_{max}} \left(\frac{\hbar\omega}{k_B T}\right)^2 \frac{e^{\hbar\omega/k_B T}}{\left[e^{\hbar\omega/k_B T}-1\right]^2}\, g(\omega)\, d\omega. \quad (2)$$

Further properties such as entropy and internal energy were evaluated by integrating $C_V(T)/T$ and $C_V(T)$ from $T = 0$ K to the desired temperature. Since the main concern was to employ these data in thermodynamic calculations performed at constant pressure, the integration was only done up to the reference temperature $T_{ref} = 298.15$ K where the $C_p$–$C_V$ difference is assumed to be negligible.

The Hellmann–Feynman forces necessary to evaluate the force constants and to build up the dynamical matrices were generated by Vienna Ab-initio Simulation Package (*VASP*) [22]. For this purpose, the $2 \times 2 \times 2$ supercells ($2 \times 2 \times 1$ for $AnAl_4$) were

constructed and two, three and twelve independent displacements of 0.03 Å were applied on the individual atoms in $AnAl_2$, $AnAl_3$ and $AnAl_4$, respectively. The FM spin polarization without S–O coupling, PBE96 [19] exchange-correlation potential, the projector augmented wave (PAW) pseudopotentials [32], plane wave basis set expanded up to the cut-off energy of 532 eV and the $3 \times 3 \times 3$ Monkhorst–Pack *k*-sampling were considered in all *VASP* calculations. Similarly to ground state calculations performed by *WIEN2k* the experimental lattice parameters were considered in calculations of Hellmann–Feynman forces.

The calculations of phase equilibria and the construction of phase diagrams were carried out by means of the *FactSage* thermochemical software and databases [33], version 6.0. The thermodynamic data for Al were taken from *FACT53* database whereas the data assessed in this study and those for actinide elements adopted from literature [20] were collected in separate *ACTIBASE* and *ACTISOL* compound and solution databases, respectively. The *CALPHAD* technique was applied for the assessment of unknown thermodynamic data considering the results of *ab-initio* calculations performed in this work, as well as the experimental calorimetry and high temperature equilibrium data discussed above.

## 3. Results and discussion

### 3.1. Ab-initio calculations

All calculated electronic structures reveal a clear spin polarization which is manifested by increasing exchange splitting of An-5*f* bands located at the Fermi level and also an increasing spin moment as the spin-up 5*f* band is gradually filled from U to Pu (see the calculated electronic structure of $PuAl_2$ in Fig. 1 as an example). The typical occupation of 5*f* states and the spin moment measured in $\mu_B$ are 2, 3.5 and 5 for U, Np and Pu, respectively. Moreover, due to S–O coupling the orbital moments oriented in the opposite direction are formed on An atoms attaining the respective values 1.3, 2.9 and 2.2$\mu_B$.

Assuming the An-5*f* orbitals are only marginally involved in chemical bond, the effective numbers of electrons the An atoms contribute to the bonding are 4, 3.5 and 3, which might be also considered as their effective valences. As a result, the cohesive energies decrease from U to Pu (the Pu compounds being the least stable) for all three series. This is a typical behavior of most light An compounds which exhibit an increasing stability from Ac to U followed by a reversal towards Pu or Am and lanthanide-like linear downtrend from Am to heavy An [34]. However, the resulting heats of formation are likewise affected by the stability of the constituent An metals, where the non-magnetic uranium with its *f*-electrons highly contributing to the chemical bond is the most stable one.

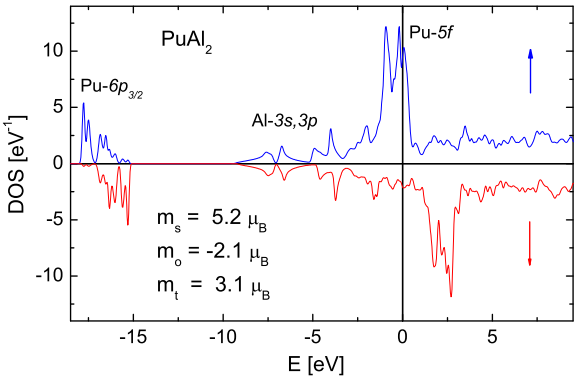


**Fig. 1.** Calculated density of states (DOS) of $PuA1_2$. Majority spin channel (↑) positive, minority spin channel (↓) negative.

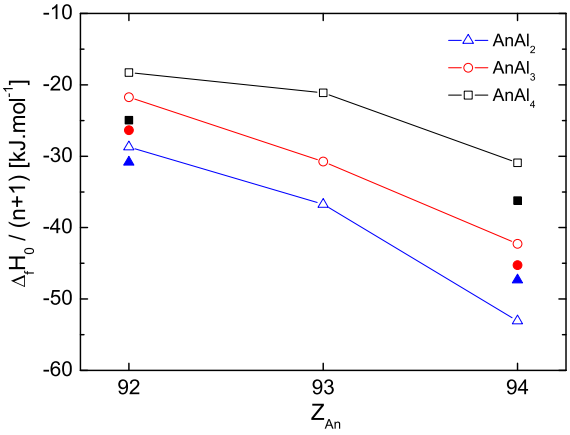


**Fig. 2.** The ground state enthalpies of formation, $\Delta_f H_0^\circ$ (referred to total number of atoms per formula unit, $n+1$), calculated by *Wien2K* (open symbols and solid lines) and compared with the experimental values [8,10] (filled symbols).

**Table 2**
Enthalpy of formation, $\Delta_f H_0^\circ$, the phonon (ph.) and electron (el.) contribution to relative enthalpy, $H_{298}^\circ - H_0^\circ$ (including zero point energy in the phonon part) and the respective contributions to entropy, $S_{298}^\circ$. The last column, $\Delta_f S_{298}^\circ$, represents the entropy of formation without magnetic part.

| | $\Delta_f H_0^\circ$ | $H_{298}^\circ - H_0^\circ$ | | $S_{298}^\circ$ | | $\Delta_f S_{298}^\circ$ |
|---|---|---|---|---|---|---|
| | kJ mol$^{-1}$ | | | J mol$^{-1}$ K$^{-1}$ | | |
| | | el. | ph. | el. | ph. | |
| $UA1_2$ | −86.1 | 0.67 | 24.2 | 4.5 | 101.2 | −1.1 |
| $NpA1_2$ | −110.2 | 0.78 | 24.2 | 5.2 | 99.5 | −2.3 |
| $PuA1_2$ | −159.2 | 0.64 | 24.1 | 4.3 | 105.3 | −1.4 |
| $UA1_3$ | −87.0 | 0.65 | 32.3 | 4.4 | 117.5 | −13.1 |
| $NpA1_3$ | −122.9 | 0.39 | 32.1 | 2.6 | 120.6 | −12.1 |
| $PuAl_3$-3H | −169.1 | 0.97 | 32.0 | 6.5 | 122.4 | −10.4 |
| $PuAl_3$-6H | −172.4 | 0.71 | – | 4.8 | – | – |
| $PuAl_3$-9H | −174.3 | 0.75 | – | 5.0 | – | – |
| $UAl_4$ | −91.4 | 1.00 | – | 5.7 | – | – |
| $NpA1_4$ | −105.6 | 0.51 | 40.5 | 3.4 | 152.1 | −8.1 |
| $PuAl_4$ | −154.7 | 0.98 | – | 6.5 | – | – |

Consequently, the enthalpies of formation shown in Fig. 2 and Table 2 reveal an opposite trend with Pu compounds being the most stable with respect to the elemental metals.

The decreasing stability from $AnAl_2$ to $AnAl_4$ is a general characteristic observed in most binary intermetallic compounds and it largely originates from the Madelung contribution to the cohesive energy. This contribution is indeed not present in pure metals which is also the cause of the exothermic values of enthalpies of formation of intermetallic compounds in general. There are two reasons why this term becomes most dominant when approaching the 1:1 ratio of the constituent elements. First, the fraction of unlike nearest neighbors reaches the maximum and, second, the absolute values of partial charges also increase towards this composition. The described trend can be demonstrated on the $PuAn_n$ series, where the average fraction of Pu nearest neighbors of an Al atom increases from 24% for $n = 4$–75% for $n = 2$. Moreover, if we assign the overall charge from the interstitial region back to the individual atoms according to the rate they attract valence electrons (measured as a fraction of valence electrons remaining in muffin-tin), we obtain the partial charges of Pu $\delta_{Pu} = -2, -1.2$ and $-1.3$ and those of Al $\delta_{Al} = +1, +0.4$ and $+0.3$ for $n = 2$, 3 and 4, respectively. The largest partial charges are thus observed for the most stable compound, $PuA1_2$. It is noteworthy that both the degree to which an atom is surrounded by dissimilar atoms, and the electronegativity difference affecting the magnitude of

partial charges appear in the original Miedemas's model for the enthalpy of formation of intermetallic compounds [35]. However, the latter term remains invariant with composition, whereas the real partial charges can vary from one compound to another and, as seen from the $PuA1_n$ example, they can contribute to higher stability of those compounds with lower $n$.

The stability of uranium and plutonium compounds expressed in terms of calculated enthalpies of formation is underestimated by 6—34 kJ mol$^{-1}$ (except for $PuA1_2$ which turns out to be more stable) compared to experimental calorimetric [8,10,11] and emf [11,4] data. The selected calorimetric data are also given in Fig. 2 for comparison. Let us note that the simple spin polarized calculations provide even less exothermic values which are improved in most cases by $\sim$ 10 kJ mol$^{-1}$ once the S–O interaction is included. When comparing the experimental and calculated results one should consider the typical uncertainty in solution calorimetry ($\sim$ 10 kJ mol$^{-1}$) [8,10] and an An sub-stoichiometry which has been reported in particular for $UAl_4$, $PuAl_3$ and $PuAl_4$ [2,3]. On the other hand, the calculated enthalpies of formation might be affected by neglecting the correlation effects going beyond the used GGA. The on-site Coulomb repulsion between An-5$f$ electrons might be indeed different in intermetallic compounds and pure metals due to a different occupation and degree of localization of these states. Although the observed discrepancy is significant with regard to the accuracy required in thermodynamic modeling, the ab-initio calculations provide a clear insight into the energetics of the compounds under study and make it possible to correlate it with the essential features of electronic structure. Moreover, the calculated results seem to be internally consistent, as it can be demonstrated on the stability of $PuAl_3$ polymorphs (Table 2) decreasing from $PuAl_3$-9H to $PuAl_3$-3H in accordance with the experimental phase diagram [3].

All calculated phonon spectra show a low frequency peak which originates from acoustic phonon branches and is predominantly contributed by vibration modes of large An atoms $\sim$(95—97%). The high frequency optical phonon bands (largely formed by Al vibration modes) are separated from the acoustic branches by a band gap of $\sim$2.5 THz width (see the phonon spectra of $NpA1_2$ and $PuA1_2$ in Fig. 3 as examples). This band gap does not appear in the $AnAl_3$ series, which also exhibits larger admixture of Al vibrations into low frequency phonons $\sim$(10%). A closer inspection of PDOS's within an isostructural series reveals a slight shift of most features of phonon spectra to lower frequencies when going from U to Pu. This effect is also apparent from the comparison of $NpA1_2$ and $PuA1_2$ (Fig. 3) and can be attributed to increasing atomic mass of An and little weaker Hellmann–Feynman forces due to softer An–Al bonds.

The observed shift to lower frequencies implies a faster saturation of lattice heat capacity with temperature towards Dulong–Petit limit and, as seen from Table 2, also a higher lattice vibration entropy and enthalpy at $T_{ref}$ = 298.15 K for heavier An. Due to a slight admixture of Al vibration states into the low frequency acoustic phonons the effective Debye temperature is higher in the intermetallic compounds compared to An metals and the corresponding $\Delta_f C_p$ is thus negative in the low temperature range which, being weighted by a factor $1/T$, decidedly contributes to the negative values of entropy of formation, $\Delta_f S^\circ_{298}$. Since the participation of Al vibrations in the low frequency spectrum is more considerable in the $AnAl_3$ series, more negative values of $\Delta_f S^\circ_{298}$ are accordingly obtained in this case. The observed trend in $\Delta_f S^\circ_{298}$ is not changed even after the electronic contribution is figured in.

However, the values of $\Delta_f S^\circ_{298}$ given in Table 2 do not involve the magnetic contribution. The most explored from the point of view of magnetic behavior are the Laves phases, $AnAl_2$. $UAl_2$ is known as a spin fluctuator with a characteristic $T^3 \cdot lnT$ term in low temperature specific heat, while $NpA1_2$ and $PuA1_2$ are ferromagnetically ordered and undergo low temperature transitions to paramagnetic state. Unfortunately, only low temperature $C_p$ data (up to 20 K) are available for $UAl_2$ and $PuA1_2$ [14,16]. The heat capacity of $NpA1_2$ has been recently measured from 3 K to room temperature by relaxation method [36]. If we subtract the calculated $C_{ph} + C_{el}$ from the experimental data, we obtain the magnetic contribution $S^\circ_{mag,298}(NpA1_2) = 7.6$ J mol$^{-1}$ K$^{-1}$. Provided the magnetic ordering is completely disrupted at room temperature, we can conclude the total entropy of formation of most $AnAl_n$ phases varies from slightly negative to slightly positive values.

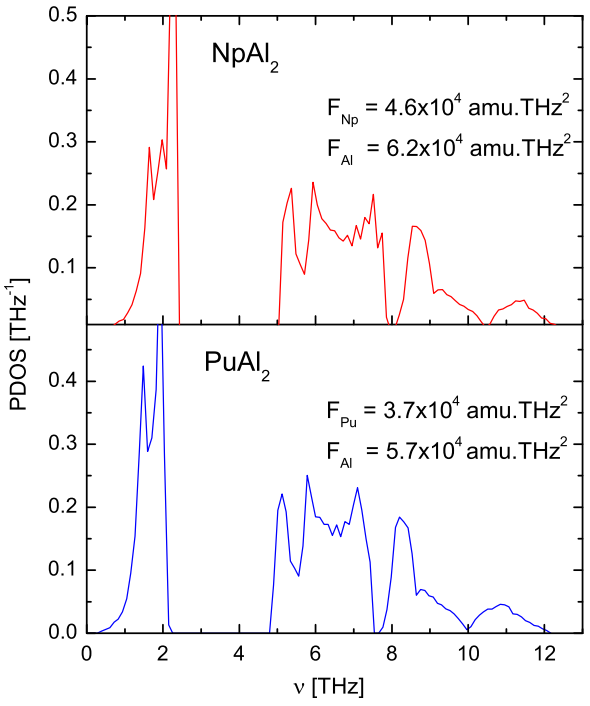


**Fig. 3.** Calculated phonon spectra of $NpA1_2$ and $PuA1_2$.

**Table 3**
Assessed values of enthalpies of formation, $\Delta_f H^\circ_{298}$, of solid stoichiometric compounds (in kJ mol$^{-1}$). The entropies of formation ar considered as zero as discussed above.

| An | $AnAl_2$ | $AnAl_3$ | $AnAl_4$ | AnAl | $An_3A1$ |
|---|---|---|---|---|---|
| U | −92.6 | −104.9 | −105.8 | | |
| Np | −112.0 | −130.8 | −133.0 | | |
| Pu | −159.2 | $-178.7^{9H}$<br>$-177.0^{6H}$<br>$-173.8^{3H}$ | −182.0 | −83.0 | −95.8 |

### 3.2. Phase diagrams

The thermodynamic models of the stoichiometric phases ($AnAl_n$, $n$ = 1, 2, 3, $Pu_3Al$ and PuAl) are based on the standard enthalpies of formation assessed in this work, which are listed in Table 3. As discussed above, the standard entropies of formation resulting from phonon and electronic structure calculations as well as from the estimated magnetic behavior are rather small and are thus considered to be zero in all cases. Similarly, the heat capacity above the ambient temperature is assumed to observe the Neumann–Kopp additivity rule (NKR) with respect to constituent metals, since the harmonic crystal approximation used in phonon calculations and the Sommerfeld model for electron excitations are not supposed to adequately describe the heat capacity at

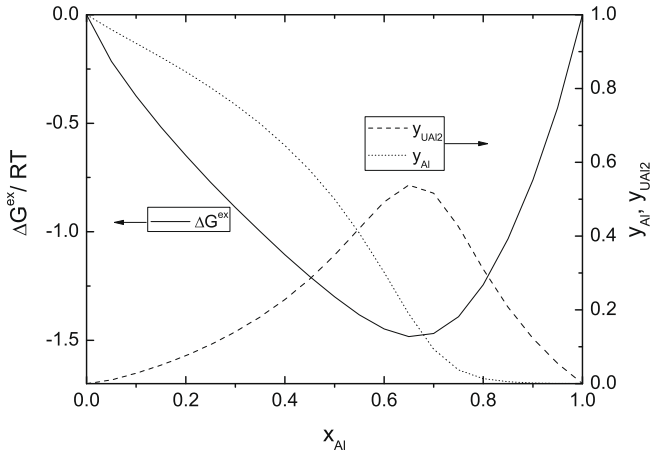


**Fig. 4.** The excess Gibbs energy of U–Al liquid, $\Delta G^{ex}$, and the mole fractions of the respective species, $y_i$ as functions of total Al concentration, $x_{Al}$ (at $T = 1500$ K).

elevated temperatures. However, as mentioned above, high temperature emf measurements performed on $UA1_n$ [11,12] and $PuA1_n$ [4,13] provide more exothermic values of $\Delta_f H^\circ$ than ambient temperature calorimetry data and also negative values of $\Delta_f S^\circ$. Qualitatively similar results are also reported for U–Al phases by Wang et al. [6] who assessed the Gibbs energies of formation from high temperature equilibrium data. These results seem to indicate a considerable negative departure from NKR at elevated temperatures. In our models on the other hand, only the enthalpies and entropies of transformation between different An-allotropes contribute to higher $\Delta_f H^\circ$ and lower $\Delta_f S^\circ$ at $T > T_{ref}$ compared to reference temperature $T_{ref} = 298.15$ K. Although an An sub-stoichiometry has been reported for both $UAl_4$ [2] and $PuAl_4$ [3] as well as for $PuAl_3$ [3], all $AnAl_n$ phases are considered as stoichiometric in this study. Let us note that the recent crystal structure refinement study brings an evidence that $UAl_4$ can be prepared as a fully stoichiometric compound with no vacancies on U-sublattice [37].

The Gibbs free energy of all solution phases is described in a standard way,

$$G^\phi = \sum_i (y_i G_i^\circ + \mathbf{R}T\, y_i ln y_i) + \Delta G^{ex}, \tag{3}$$

as a sum of Gibbs energies of the involved species $G_i^\circ$, the ideal entropy term and the excess Gibbs energy considered in a simple polynomial form

$$\Delta G^{ex} = \sum_{M \neq N} \sum_{ij} L_{ij(M,N)} \cdot y_M^i y_N^j. \tag{4}$$

The liquid phase is expressed in terms of associate solution model with two liquid end-members, An(l) and Al(l), and a single associate, $AnAl_2$(l), which effectively describes a considerable negative deviation from ideality at this composition, as demonstrated for the excess Gibbs energy of U–Al liquid (Fig. 4). Due to a lack of experimental information needed for an assessment, the model parameters for Np–Al liquid were evaluated by linear interpolation between the respective parameters used for U–Al and Pu–Al.

In addition to the liquid phase, four solid solutions based on different An-allotropes, namely $\gamma$-U, $\gamma$-Np, $\epsilon$-Pu and $\delta$-Pu were considered. While the former three are modeled as solutions of elemental end-members with Al adopting the same structure as the respective An (bcc, $Im\bar{3}m$), the $\delta$-Pu solution turned out to be better described as a mixture of $\delta$-Pu and the cubic form of $Pu_3Al$, where the latter end-member was considered as fcc structure with 1/4 of Al substituting Pu in an ordered way ($Pm\bar{3}m$). Topologically it has the same structure as the line compound $Pu_3Al$, which is however tetragonally distorted ($P4mmm$). All assessed parameters appearing in the models for solution phases are summarized in Table 4.

**Table 4**
Assessed model parameters of solution phases (enthalpies of formation, $\Delta_f H^\circ_{298}$, and interaction parameters, $L_{ij}$, in kJ mol$^{-1}$, entropies, $S^\circ_{298}$, and heat capacities, $C^\circ_p$, in J mol$^{-1}$ K$^{-1}$).

| | | | |
|---|---|---|---|
| *Liquids* | | | |
| U–Al | $UA1_2$(l): | $\Delta_f H^\circ_{298} = -19.8$ | $S^\circ_{298} = 119$ |
| | | | $C^\circ_p = 112$ |
| | | $L_{21(U,UAl_2)} = 18$ | $L_{21(Al,UAl_2)} = -12$ |
| Np–Al | $NpA1_2$(l): | $\Delta_f H^\circ_{298} = -48.7$ | $S^\circ_{298} = 128$ |
| | | | $C^\circ_p = 109$ |
| | | $L_{21(Np,NpAl_2)} = 9$ | $L_{21(Al,NpAl_2)} = -23$ |
| | | $L_{11(Np,NpAl_2)} = 8.5$ | |
| Pu–Al | $PuA1_2$(l): | $\Delta_f H^\circ_{298} = -79.2$ | $S^\circ_{298} = 140$ |
| | | | $C^\circ_p = 106$ |
| | | $L_{11(Pu,UAl_2)} = 17$ | $L_{21(Al,PuAl_2)} = -34$ |
| *Solid solutions* | | | |
| | Al(bcc)[a]: | $\Delta_f H^\circ_{298} = 10.1$ | $S^\circ_{298} = 32.5$ |
| $\gamma$-U | | $L_{11(U,Al)} = -12$ | |
| $\gamma$-Np | | $L_{11(Np,Al)} = -12$ | |
| $\delta$-Pu | $Pu_3Al$: | $\Delta_f H^\circ_{298} = -75.0$ | $S^\circ_{298} = 202$ |
| | | $L_{11(Pu,Pu_3Al)} = -10$ | |
| $\epsilon$-Pu | | $L_{11(Pu,Al)} = 68$ | $L_{21(Pu,Al)} = -136$ |

[a] SGTE value from SGPS (pure substances) database comprised in *FactSage* 6.0 [33], used for $\gamma$-U, $\gamma$-Np and $\epsilon$-Pu.

The assessment was performed starting from the calorimetry and/or ab-initio enthalpy of formation of $AnAl_2$ which is the most stable compound in all three systems. The temperature of its congruent melting [2,3] was first optimized by varying the enthalpy and temperature of virtual congruent melting to a liquid $AnAl_2$ associate. In the next step, the parameters of the excess Gibbs energy of the melt and heats of formation of $AnAl_3$ and $AnAl_4$ were changed by trial and error in order to reproduce the experimental temperatures of peritectic melting of these two compounds [2,3]. The assessed and experimental enthalpies of formation are generally in good accordance except for $UAl_4$ where the difference exceeded 20 kJ mol$^{-1}$ (the experimental value is $\sim$−127 kJ mol$^{-1}$ [8,11]). On the other hand, the calculated enthalpies of formation are in general less exothermic compared to the assessed ones. As a result of the used assessment strategy the difference is quite small for $AnAl_2$, but increases towards $AnAl_4$ reaching the average values 8 and 23 kJ mol$^{-1}$ for $AnAl_3$ and $AnAl_4$, respectively. This would either suggest a sharper minimum in the excess Gibbs energy of the liquid phase or temperature dependent excess parameters. The model parameters of the solid solutions derived from the An metals and the enthalpies of formation of PuAl and $Pu_3Al$ were eventually optimized based on the experimental data given in Kassner's et al. compilations [2,3] (see Figs. 5 and 6 for comparison).

The calculated phase diagrams are shown in Figs. 5–7. A satisfactory agreement between the experimental and calculated temperatures of invariant points was achieved in U–Al (Fig. 5) and Pu–Al (Fig. 6) system. As the experimental liquidus data were not considered during the assessment, the calculated liquidus curve in Al rich part does not fully fit the experimental points in U–Al system, so that the peritectic composition of $UA1_3$ is slightly shifted towards An while the $UAl_4$-Al eutectics is closer to Al. Since the experimental information is very scarce in Np–Al system, the calculated phase diagram in Fig. 7 based on the interpolation of liquid behavior between U–Al and Pu–Al and on ab-initio enthalpies of formation of $NpA1_n$ should be considered as a tentative picture of the phase relations in this system.

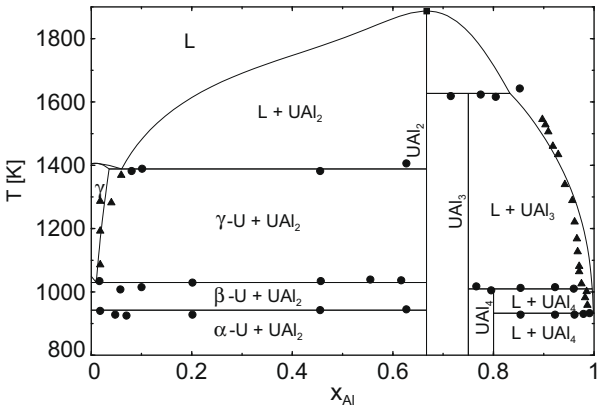


**Fig. 5.** Calculated phase diagram of U–Al system. Experimental data points (solid symbols) are taken from [2].

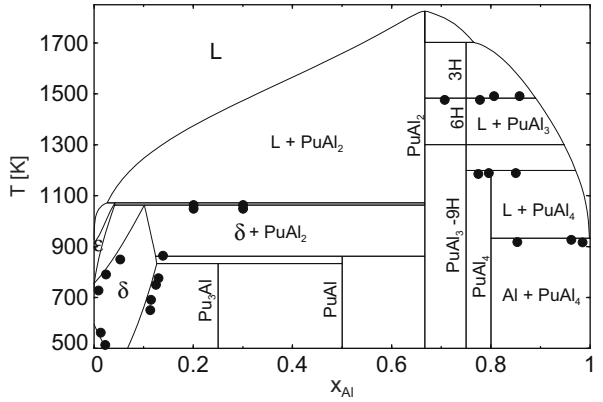


**Fig. 6.** Calculated phase diagram of Pu–Al system. Experimental data points (solid symbols) are taken from [3].

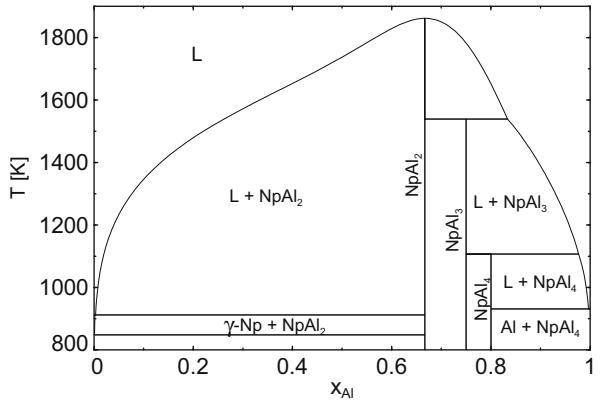


**Fig. 7.** Calculated phase diagram of Np–Al system. Only a minute amount of Al is dissolved in $\gamma$-Np.

## 4. Conclusions

Thermodynamic properties of actinide–aluminium compounds, which are involved in the pyrochemical reprocessing technique of spent nuclear fuels, were studied by both first principle calculations and thermodynamic data evaluation based on *CALPHAD* approach. The stability of the studied compounds as predicted by full potential plane wave calculations is in general slightly underestimated compared to available experimental and assessed heats of formation. This effect has been ascribed to higher order correlation effects not involved in the used GGA functional. Despite this discrepancy the DFT calculations provided an insight into the cohesive characteristics and made it possible to interpret the observed trends along the An-series.

Moreover, the main contributions to the entropy arising from lattice vibrations and conduction electron excitations were evaluated from calculated phonon spectra and electronic density states, respectively. By adding the estimated magnetic entropy, the total entropy of formation turns out to be close to zero. Hence, the highly negative entropies of formation as derived from high temperature equilibrium measurements based on second law must be interpreted in terms of large negative deviation from Neumann–Kopp rule at elevated temperatures. The high temperature heat capacity measurements would be thus highly needed.

Last, based on the observed and anticipated trends in thermochemical properties from uranium to plutonium the phase diagram of Np–Al system is presented for the first time along with the (re-)assessed U–Al and Pu–Al phase diagrams.

## Acknowledgement

D.S. greatly acknowledges the European Commission for support in the frame of the Program "Training and mobility of researchers". A part of this work was supported by the Ministry of Education of Czech Republic, Project No. MSM6046137302.

## References

[1] J. Serp, M. Allibert, A. LeTerrier, R. Malmbeck, M. Ougier, J. Rebizant, J.-P. Glatz, J. Electrochem. Soc. 152 (2005) 167.
[2] M. Kassner, M. Adamson, P. Adler, D. Peterson, Bull. Alloy Phase Diag. 11 (1) (1990) 82.
[3] M. Kassner, D. Peterson, Bull. Alloy Phase Diag. 10 (4a) (1989) 459.
[4] P. Chiotti, V. Akhachinski, I. Ansara, M. Rand, in: The Chemical Thermodynamics of Actinide Elements and Compounds, Part 5, IAEA, 1981, p. 231.
[5] F. Ellinger, W. Miner, D. O'Boyle, F. Schonfeld, Constitution of Plutonium Alloys, Tech. Rep. LA-3870, Los Alamos National Laboratory, 1968.
[6] J. Wang, X. Liu, C. Wang, J. Nucl. Mater. 374 (2008) 79.
[7] O. Runnalls, Trans. Am. Inst. Min., Metall. Petrol. Eng. 197 (1953) 1460.
[8] M. Ivanov, M. Tumbakov, N. Podol'skaya, Atom. Energy 5 (1958) 166.
[9] K. Nagarajan, R. Baba, C. Mathews, J. Nucl. Mater. 201 (1993) 142.
[10] V. Akhachinski, L. Kopyten, M. Ivanov, N. Podol'skaya, Heat of formation of intermetallic compounds of plutonium with aluminium and iron and of uranium with iron, in: Thermodynamics of Nuclear Materials – Proc. Int. Symp., IAEA, 1962, p. 309.
[11] P. Chiotti, J. Kateley, J. Nucl. Mater. 32 (1969) 135.
[12] V. Lebedev, Sal'nekov, I. Nichkov, S. Paspopin, Sov. J. Atom. Energy 32 (1972) 129.
[13] V. Lebedev, V. Kober, V. Sal'nekov, G. Kazantsev, I. Nichkov, S. Paspopin, O. Skiba, V. Efremov, Sov. RadioChem. 18 (1976) 113.
[14] R. Trainor, M. Brodsky, H. Culbert, Phys. Rev. Lett. 34 (1975) 1019.
[15] V. Stobyarov, L. Danelyan, L. Prokof'eva, Sov. Phys. Solid State 28 (1986) 1384.
[16] G. Stewart, R. Elliott, Phys. Rev. B 31 (1985) 4669.
[17] D. Aoki, Y. Haga, Y. Homma, Y. Shiokawa, E. Yamamoto, A. Nakamura, R. Settai, Y. Onuki, J. Phys. Soc. Jpn. 78 (2009) 044712.
[18] P. Blaha, K. Schwarz, G. Madsen, D. Kvasnicka, J. Luitz, WIEN2k, An Augmented Plane Wave + Local Orbitals Program for Calculating Crystal Properties, Karlheinz Schwarz, Techn. Universität Wien, Austria, 2001.
[19] J. Perdew, S. Burke, M. Ernzerhof, Phys. Rev. Lett. 77 (1996) 3865.
[20] R. Guillaumont, T. Fanghänel, J .Fuger, I. Grenthe, V. Neck, D. Palmer, M. Rand, Update on the Chemical Thermodynamics of U, Np, Pu, Am and Tc, Elsevier, 2003.
[21] K. Parlinski, Softw. Phonon (2006).
[22] G. Kresse, J. Furthmüller, Phys. Rev. B 54 (1996) 11169.
[23] G. Katz, A. Jacobs, J. Nucl. Mater. 5 (1962) 338.
[24] O. Runnalls, J. Metals 5 (1953) 1460.
[25] O. Runnalls, J. Nucl. Mater. 5 (2) (1962) 165.
[26] G. Petzow, H. Exner, A. Chakraborty, J. Nucl. Mater. 25 (1968) 1.
[27] A. Mitchell, D. Lam, J. Nucl. Mater. 52 (1974) 125.
[28] O. Runnalls, R. Boucher, J. Nucl. Mater. 15 (1965) 57.
[29] O. Runnalls, R. Boucher, Acta Crystallogr. 19 (1965) 184.
[30] V. Zenou, G. Kimmel, C. Cotler, M. Aizenshtein, J. Alloys Compd. 329 (2001) 189.
[31] O. Runnalls, Can. J. Chem. 34 (1956) 133.

[32] G. Kresse, J. Joubert, Phys. Rev. B 59 (1999) 1758.
[33] C. Bale, P. Chartrand, S. Degterov, G. Eriksson, Hack, R. BenMahfoud, J. Melanton, A. Pelton, S. Petersen, Calphad 26 (2) (2002) 189.
[34] D. Sedmidubský, R. Konings, Novák, J. Nucl. Mater. 344 (2005) 40.
[35] F. de Boer, R. Boom, W. Mattens, A. Miedema, A. Niessen (Eds.), Cohesion in Metals, North-Holland, Amsterdam, 1988 (Ch. Transition Metal Alloys).
[36] J.-C. Griveau, E. Colineau, unpublished 2008.
[37] O. Tougait, H. Noël, Intermetallics 12 (2004) 219.